Scalable nonlinear helical dichroism in chiral and achiral molecules

Jean-Luc Bégin (jbegi038@uottawa.ca)
University of Ottawa
Ashish Jain
University of Ottawa
Andrew Parks
University of Ottawa
Felix Hufnagel
University of Ottawa
Paul Corkum
University of Ottawa
Ebrahim Karimi
University of Ottawa https://orcid.org/0000-0002-8168-7304
Thomas Brabec
University of Ottawa
Ravi Bhardwaj
University of Ottawa

Article

Keywords:

Posted Date: May 23rd, 2022

DOI: https://doi.org/10.21203/rs.3.rs-1642827/v1

Additional Declarations: There is **NO** Competing Interest.

Version of Record: A version of this preprint was published at Nature Photonics on November 28th, 2022.
See the published version at https://doi.org/10.1038/s41566-022-01100-0.

Scalable nonlinear helical dichroism in chiral and achiral molecules

Jean-Luc Bégin[1,+], Ashish Jain[1,+], Andrew Parks[1], Felix Hufnagel[1], Paul Corkum[1], Ebrahim Karimi[1], Thomas Brabec[1], and Ravi Bhardwaj[1,*]

[1]Department of Physics, University of Ottawa, Ottawa, ON, K1N 6N5, Canada
[*]ravi.bhardwaj@uottawa.ca
[+]These authors contributed equally to this work

ABSTRACT

Chiral interactions are prevalent in nature, driving a variety of bio-chemical processes. Discerning the two non-superimposable mirror images of a chiral molecule, known as enantiomers, requires interaction with a chiral reagent with known handedness. Circularly polarized light beams are often used as a chiral reagent. Here, we demonstrate efficient chiral sensitivity with linearly polarized helical light beams carrying an orbital angular momentum of $\pm l\hbar$, in which the handedness is defined by the twisted wavefront structure tracing a left- or right-handed corkscrew pattern as it propagates in space. By probing nonlinear optical response, we show that helicity dependent nonlinear absorption occurs even in achiral molecules and can be precisely controlled. We model this effect by considering induced multipole moments in light-matter interactions. Design and control of light-matter interactions with helical light opens new opportunities in chiroptical spectroscopy, light-driven molecular machines, optical switching, and in-situ ultrafast probing of chiral systems and magnetic materials.

Introduction

Our understanding of light-matter interactions is mainly based on the propagation of homogeneously polarized light and the dominance of the dipole-active transitions between different quantum states of matter. The higher-order multipole effects are often ignored. The strength of dipole transitions is governed by the frequency, intensity and polarization of the incident light. The optical phase, represented by the wavefront of the light beam, plays a minimal role in such transitions. Within the dipole approximation, chiral systems are often studied using circularly polarized light, in which the dynamical rotation of the electric field vector around the propagation direction yields an effective Spin Angular Momentum (SAM) $\pm\hbar$, therefore the handedness. Two distinct optical techniques are widely used; Circular Dichroism (CD) and Photo-Electron Circular Dichroism (PECD). In CD, left- and right-circularly polarized light interact differently with the enantiomers leading to differential absorption[1,2]. Chiral sensitivity of CD is poor, on the order of 0.01–1%[3], because it involves coupling of electric and magnetic dipole transitions. CD can be enhanced by employing super chiral light[4], plasmonic structures[5,6], and strong field techniques using elliptically polarized light[7,8]. In PECD, photo-ionization of a chiral molecule results in an asymmetric photo-electron angular distribution that is identical but opposite in sign for the two enantiomers[9]. PECD is due to pure electric dipole transitions, therefore, its efficiency is one to two orders of magnitude larger than CD[3,10].

Light can also carry Orbital Angular Momentum (OAM) of $\pm l\hbar$ associated with dynamical rotation of wavefront structure[11–13]. The handedness of such helical light beams is defined by the twisting of the wavefront undergoing l rotations in one wavelength. This additional degree of freedom influences the characteristics of light-matter interactions. The angular distribution[14], time delay[15], and dynamics of photo-electrons[16,17] can be modified during the photo-ionization of atoms and molecules. Also, the OAM of light can be transferred to matter either externally by exerting a torque (as demonstrated in optical tweezers[18], atomic clouds and Bose-Einstein condensates[19,20]) or internally by rotating the electron distribution resulting in modified selection rules for transitions between two quantum states that depend on topological charge l[21,22].

The possibility of no upper bound on l value, while SAM can assume only two defined values, generated significant interest in using helical light beams carrying OAM as a chiral reagent. Early studies on chirality with twisted photons were not promising. Most experiments were performed in the linear absorption regime[23,24] while theory focused solely on the coupling of electric and magnetic dipole transition moments responsible for conventional CD[25]. Helical Dichroism (HD), the analogous of CD, was demonstrated only in nanoparticle aggregates[26] by exploiting local field enhancements to discriminate the enantiomers, and in chiral metasurfaces[27] . Coupling of OAM of light with material's chirality without any intermediary was recently shown to require the higher-order transition moments to be engaged along with SAM to observe any chiroptical effects[28,29].

In this article, we introduce conceptually new form of chiroptical detection technique based on nonlinear absorption of linearly polarized helical light beams, in liquid phase. First, we demonstrate enantio-selectivity directly without any intermediary. Second, we show helicity-dependent nonlinear absorption in molecules (chiral and achiral) that scales linearly with OAM value and can be precisely controlled. This unique feature does not exist in polarization based chiroptical techniques, such as CD. We show HD, defined as differential absorption of left- and right-handed helical light, is a phase effect and does not necessarily require circularly polarized light. To understand HD, we model light-matter interaction by considering multipole expansion. We find HD to arise from the coupling of the electric dipole and electric quadrupole terms, and can be tuned by changing the laser polarization in addition to the OAM value.

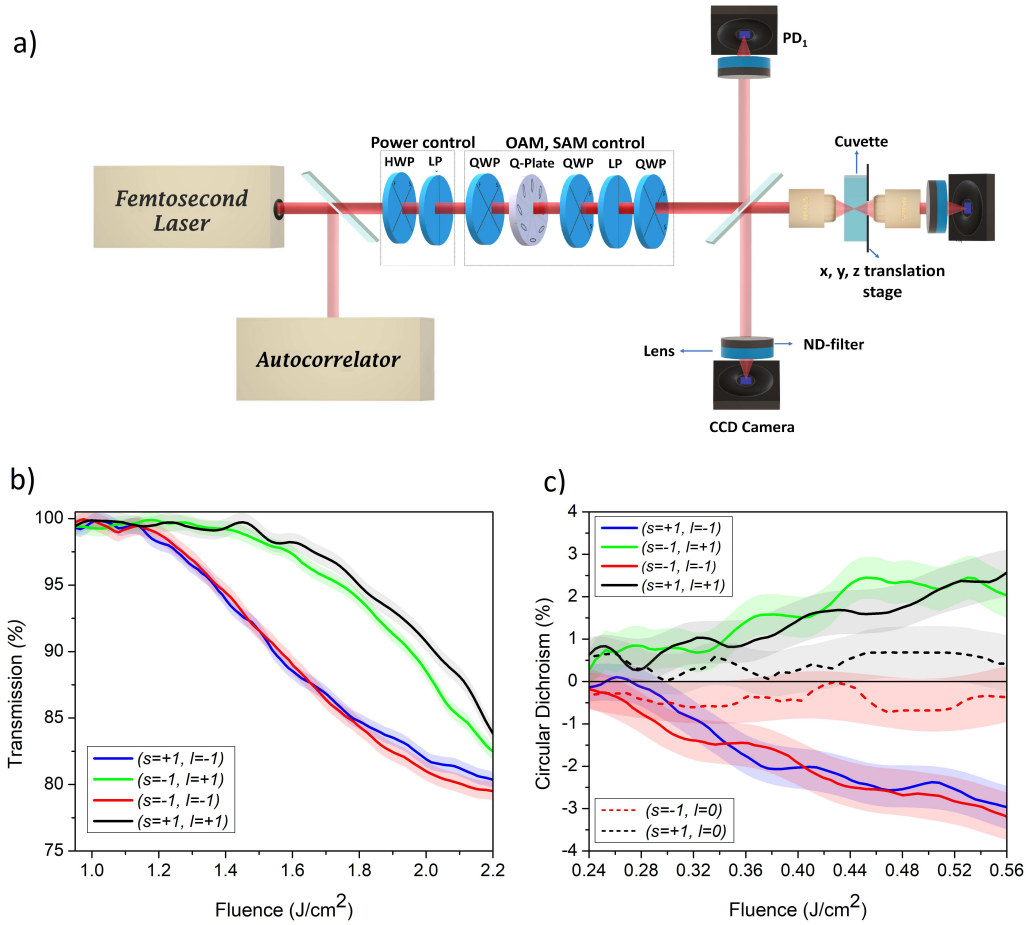

Figure 1. Transmission of circularly polarized ($s = \pm 1$) femtosecond vortex pulses in S(+)-fenchone. **(a)** Schematic of the experimental setup (see Methods for details). **(b)** Transmission of left and right circularly polarized helical light with $l = \pm 1$ in fenchone as a function of fluence. **(c)** Circular dichroism in fenchone with Gaussian ($l = 0$, dashed lines) and OAM ($l = \pm 1$, solid lines) beams as a function of fluence of a Gaussian beam. For $l = \pm 1$, the fluence needs to be scaled up by a factor of 4.3[30]. The color bands represent the statistical propagation of error.

To probe dichroism, we measured the absorption of loosely focused femtosecond Gaussian and helical light pulses propagating through a liquid sample contained in a cuvette, as shown in Fig. 1a. A q-plate converted incident Gaussian to Optical Vortex Beam (OVB) carrying an OAM value that is two times the topological charge, q[31,32]. Further experimental details are provided in the Methods section. Normalized transmission of left and right-circularly polarized ($s = \pm 1$) helical light ($l = \pm 1$) is shown in Fig.1b as a function of laser fluence in S(+)-fenchone, $C_{10}H_{16}O$. For each successive laser pulse, the energy was varied using a combination of half-wave plate and polarizer, and a fresh sample region was irradiated by translating the cuvette. Each curve in the figure is an average of three independent measurements, and the color band represents the statistical standard error. At low laser fluences, all four transmission curves overlap. Absorption is negligible since the laser fluence is not sufficient enough to induce multi-photon transitions. At the onset of multi-photon absorption ($\sim$1.2 J/cm^2), the

transmission starts to decrease monotonically. For a given helicity, transmission is nearly identical for left- and right-circularly polarized light except at fluences greater than ~1.8 J/cm^2. Similar results were obtained for chiral molecule limonene, $C_{10}H_{16}$.

CD signal in fenchone, defined as CD($l = \pm 1; s = \pm 1$) = 2 $\frac{D(\pm l;\pm s)-L(\pm l;\pm s)}{D(\pm l;\pm s)+L(\pm l;\pm s)}$ *(see Methods for notation)*, is shown in Fig. 1c for both Gaussian (dashed lines) and helical light (solid lines). For a Gaussian beam, CD is less than 1%. Overlap of chiral signal with the statistical error bands represents the sensitivity of our experiment. The chiral signal is enhanced significantly when the helical phase is introduced to the incident beam by switching from Gaussian to OAM beam. For $l = \pm 1$, the CD is about 5%. However, SAM associated with light polarization appears to play a minimal role in CD. For a given helicity, CD for left- and right circularly polarized light nearly overlap with each other within the experimental errors similar to the Gaussian beam.

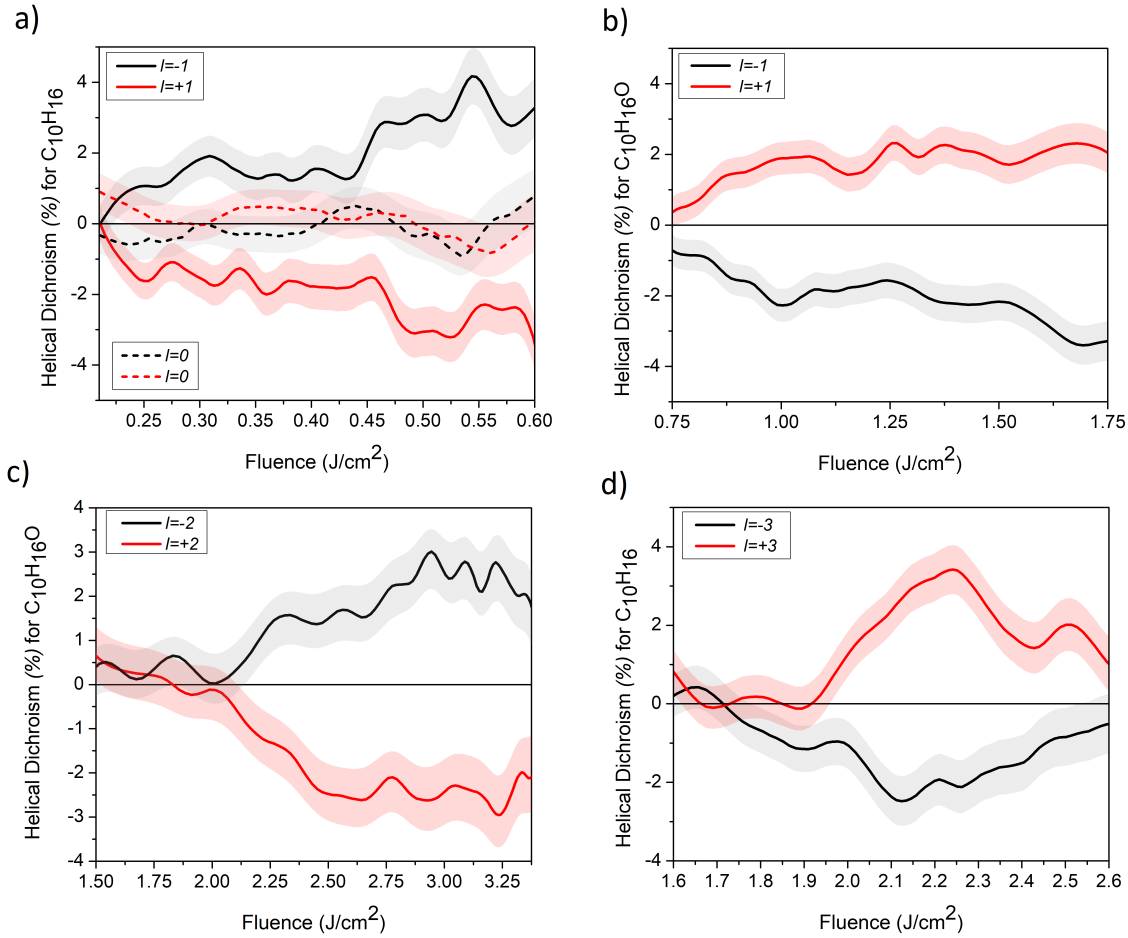

Figure 2. Helical dichroism in chiral molecules with linearly polarized light ($s = 0$) as a function of fluence. (a) Limonene with helical ($l = \pm 1$, solid lines) and Gaussian beams ($l = 0$, dashed lines). The fluence shown is for $l = 0$ and needs to be scaled by a factor of 4.3 for $l = \pm 1$. **(b), (c)** Fenchone with helical light $l = \pm 1$. and $l = \pm 2$, respectively. **(d)** Limonene with $l = \pm 3$.

To isolate the role of SAM and OAM, we performed experiments with linearly polarized ($s = 0$) helical ($\pm l$) and Gaussian beams in limonene and fenchone (Fig. 2). Helical dichroism was defined as HD($\pm l, s = 0$) = 2 $\frac{D(\pm l)-L(\pm l)}{D(\pm l)+L(\pm l)}$ to represent the chiral signal. Figures 2a, 2b show HD in limonene and fenchone, respectively, as a function of fluence for $l = \pm 1$. Also shown in Fig. 2a is differential absorption of two orthogonal linearly polarized Gaussian beams (dashed lines). The chiral signal increases with laser fluence in both molecules and reaches a maximum of ~ 4-6%. The HD signals in limonene and fenchone are of opposite signs (black curve and red curves are flipped) because they rotate the plane of linear polarization in opposite directions *(see Methods)*. The HD signal in fenchone (Fig. 2b, 2c) increased with the helicity (l value) of the beam, but did not scale up in limonene (Fig. 2a,d). Chiral discrimination with linearly polarized helical light beams demonstrates the prominent role of the optical phase associated with OAM of light.

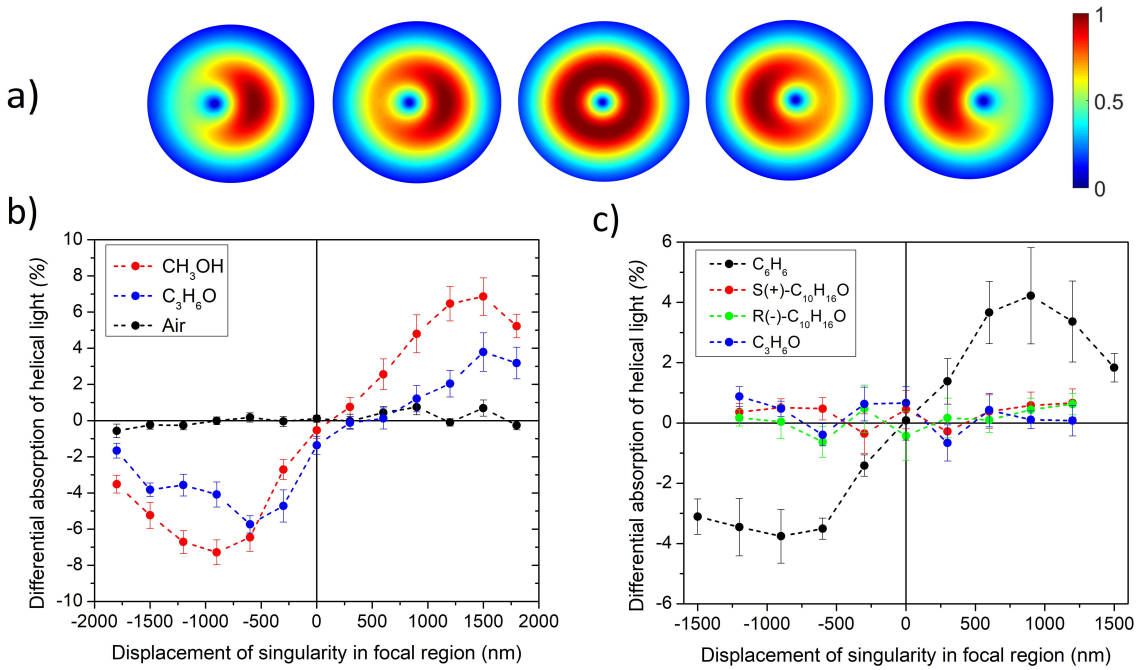

Figure 3. Helicity-dependent absorption in achiral molecules. (a) Simulated intensity profiles of asymmetric OAM beams obtained by shifting the position of the q-plate with respect to the incident beam. Differential absorption of linearly polarized left- and right-helical light ($l = \pm 1$) as a function of displacement of the singularity in the focal region **(b)** in air (black) and in achiral molecules with no inversion symmetry - acetone (blue), methanol (red). **(c)** benzene (black) - an achiral molecule with inversion symmetry. Also shown is differential absorption of circularly polarized non-OAM beam ($l = 0$) with a singularity at the center in acetone (blue) and R(-)- and S(+)-fenchone (green and red).

Generally, dichroism (*i.e.* differential absorption) is not expected in achiral molecules with circularly polarized light. This is also true even with helical light[27]. We did not observe any differential absorption of linearly polarized helical light associated with symmetric OAM beams where the null intensity region due to phase singularity is at the center of the beam. However, when the singularity in the OAM beam is displaced from the center, achiral molecules with different point group symmetries exhibit dichroism (Fig. 3). The singularity within the focal region of a focused OAM beam can be shifted either by (a) detuning the q-plate leading to a superposition of the incident Gaussian beam with the converted OAM beam[33], or (b) physically shifting the center of the q-plate with respect to the incident beam. We used the latter technique because the former gives rise to a Gaussian component in the transmitted beam. The resultant asymmetric OAM beam introduces an asymmetry in the intensity profile in the focal region, as shown in Fig.3a. In the experiment, alignment of the singularity at the center of the OAM beam can only be defined before the objective, which translates to an uncertainty $\sim \pm 100$ nm at the focus (see Methods for calibration).

Fig.3b shows differential absorption of linearly polarized helical light ($l = \pm 1$) in achiral molecules with no inversion symmetry - acetone (C_3H_6O), methanol(CH_3OH) and air - for different positions of the singularity in the focused OAM beam. Differential absorption is averaged over a fluence range from the onset of nonlinear absorption (which depends on ionization potential) in the normalized transmission curve to $\sim 1.8 J/cm^2$ (as in fig.1b). In acetone (blue curve) and methanol (red curve), differential absorption exhibits a sinusoidal behaviour with a change in sign as the singularity traverses the zero-position from -1.8μm to 1.8μm. The small variation in the zero-crossing point for the two molecules ($\sim$ 100nm) is due to uncertainty in the position of the singularity. The dashed lines connecting the discrete experimental points are for visualization only. Helicity-dependent absorption does not exist in air (empty cuvette in the experiment) and is independent of the position of the singularity (black curve). This represents the background noise introduced by our experimental setup (*see Supplementary section 5*).

Helicity dependent absorption in benzene (C_6H_6), a molecule with inversion symmetry, is shown in Fig. 3c (black curve). The observed behaviour is similar to non-centrosymmetric molecules (Fig. 3b), suggesting that HD signal is invariant to molecular symmetry.

To disentangle the roles of phase and field gradients in an asymmetric OAM beam, we studied differential absorption of

circularly polarized, non-OAM, annular beam that mimics the profile of a Laguerre-Gaussian (LG) beam with zero OAM value (*see methods and supplementary section 6*). Dichroism in R(-)-fenchone (green curve), S(+)-fenchone (red curve) and acetone (blue curve) is independent of the position of the singularity and is less than 1%, within the standard error. Absence of differential absorption confirms that helicity-dependent absorption in achiral molecules is a phase effect and not due to field gradients.

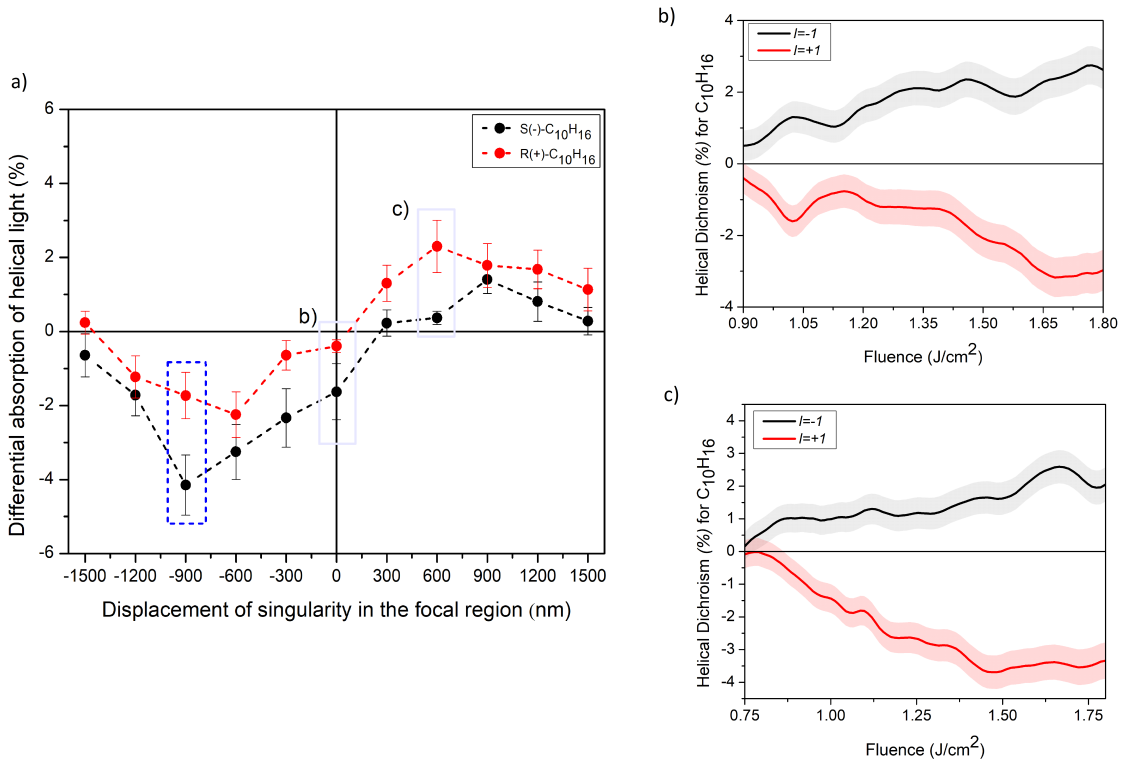

Figure 4. Helical dichroism with asymmetric OAM beams in limonene. (a) Differential absorption of linearly polarized helical light $l = \pm 1$ as a function of the position (or displacement) of the singularity in the OAM beam. **(b), (c)** Helical dichroism as a function of fluence when the singularity is at the positions marked by solid rectangles at b) and c). The blue dotted rectangle represents the position of the singularity at which the Fig. 2a was obtained.

Figure 4 shows that the HD signal in chiral molecules is weakly dependent on the position of the singularity within the OAM beam. The spatial variation of differential absorption of linearly polarized helical light in limonene enantiomers, shown in Fig. 4a, exhibits the same behaviour as achiral molecules (Fig. 3b,c). The key difference is that with the singularity displaced at the experimental center of the focused OAM beam, the helicity-dependent absorption in the two enantiomers is different, resulting in non-zero chiral signal given by HD. Figures 4b,c represent HD(%) as a function of fluence when the singularity is at the positions marked by solid rectangles in Fig. 4a. The blue dotted rectangle represents the position of the singularity at which Fig.2a was obtained. Similar results were obtained for fenchone (*see Supplementary section 1*). HD signal is not affected by the location of the phase singularity but is much more stable with asymmetric OAM beam. The results were also found not to depend on the laser focus position inside the cuvette. The effects of propagation of intense light pulses through the sample were negligible *(see Supplementary section 4)*.

To understand chiral light-matter interaction, we consider a monochromatic electromagnetic field incident on a molecule. The resultant time-harmonic charge and current distributions are described by a multipole expansion. The rate of excitation of the molecule was expressed in terms of time-averaged induced multipoles *(see Methods)*

$$\Gamma_{\delta}^{\pm} = \frac{\omega}{2}\{\underbrace{\alpha''|\tilde{E}_{\delta}^{\pm}|^2}_{\text{E1E1}} + \underbrace{\chi''|\tilde{B}_{\delta}^{\pm}|^2}_{\text{M1M1}} + \underbrace{\rho G' \text{Im}\left[(\tilde{E}_{\delta}^{\pm})^* \cdot \tilde{B}_{\delta}^{\pm}\right]}_{\text{E1M1}} + \underbrace{\frac{2}{3}\rho A'' \text{Re}\left[(\tilde{E}_{\delta}^{\pm})^* \cdot \nabla \tilde{E}_{\delta}^{\pm}\right]}_{\text{E1E2}}\} \quad (1)$$

where, ω is the frequency of incident light, E and B are incident electric and magnetic fields, α'' represents the electric polarizability, χ'' is the magnetic susceptibility, G' represents the isotropic mixed electric-magnetic dipole polarizability, A'' is

the mixed electric dipole electric quadrupole polarizability, and ρ is the orientation-dependent weighting factor for anisotropic averaging (ρ=0 for random orientations and ρ=1 for full alignment of molecules). The δ is the asymmetrical parameter, $\delta = 0$ for a symmetric LG beam and $\delta \neq 0$ for asymmetric LG beam. The sign in $\Gamma^{\pm}$ represents the sign of OAM. Derivation of equation 1 is provided in the Methods section and generalized to multiphoton absorption in Supplementary (*section 9*). E1 and M1 are electric and magnetic dipole, respectively, and E2 is the electric quadrupole. The coupling terms E1M1 and E1E2 are pseudoscalars and change sign under improper rotation. For a specific chiral system, the sign change of these quantities upon reflection would lead to non-zero differential absorption defined by

$$\Delta W = \int_{-\omega_0}^{\omega_0} \text{HD(Type I, II)} dxdy \tag{2}$$

and integrated over the beam cross-section. HD(Type I) is defined as the difference between absorption of left and right-handed helical light for the same molecule (Fig. 3, 4a)

$$\text{HD}_{\delta}(\text{Type I}) = \Gamma_{\delta}^{+} - \Gamma_{\delta}^{-} = G'[C^{+} - C^{-}] + A''[\Upsilon^{+} - \Upsilon^{-}] \tag{3}$$

HD(Type II) is defined as the difference in absorption between the two enantiomers of a chiral molecule for a specific helicity and polarization (Fig. 2, 4b,c)

$$\text{HD}_{\delta}^{\pm}(\text{Type II}) = \Gamma_{R}^{\pm} - \Gamma_{S}^{\pm} = C^{\pm}[G'_{R} - G'_{S}] + \Upsilon^{\pm}\left[A''_{R} - A''_{S}\right] \tag{4}$$

where R and S represent the two enantiomers. The parameter $\text{C}^{\pm} = 2\omega\text{Im}\left[\left(\tilde{E}_{\delta}^{\pm}\right)^{*} \cdot \tilde{B}_{\delta}^{\pm}\right]$ in Eq. (3) and (4), is called optical chirality, a local measure of the degree of circular polarization, and we define $\Upsilon^{\pm} = \frac{2\omega}{3}\text{Re}\left[\left(\tilde{E}_{\delta}^{\pm}\right)^{*} \cdot \nabla\tilde{E}_{\delta}^{\pm}\right]$ as optical helicity. Both are time-even psuedoscalars. Optical chirality is often used to describe the phenomenon of circular dichroism in molecules[4,34,35] and metasurfaces[27,36,37]. Optical helicity, Υ, is a quantity describing the handedness of helical light. It contains the gradient of the electric field giving rise to a linear l dependence. The above equations, assuming full molecular alignment, show that chiral light-matter interaction depends on both molecular transitions (contained in G' and A'') and optical chirality, C, and optical helicity, Υ.

The following qualitative behaviour emerges by evaluating Eq. (2) and (3) for HD (Type I), and Eq. (2) and (4) for HD (Type II):

- HD(Type I) is a beam-dominated property and does not exist for symmetric LG beams. For asymmetric LG beams E1M1 term vanishes (because we take the difference between left and right helical beams for the same polarization) and E1E2 coupling term is non-zero. For a circularly polarized Gaussian beam E1M1 term is non-zero and gives rise to the conventional circular dichroism.
- HD(Type II) is a material-dominated property where both E1M1 and E1E2 coupling terms contribute to differential absorption for asymmetric LG beams. For symmetric LG beams, E1E2 term averages out to zero, but the E1M1 term is non-zero and can contribute to HD. E1M1 and E1E2 are of similar magnitudes[35,38]. For asymmetric LG beams with same polarization but different helicities, the E1E2 term is responsible for the change in the sign of the HD curves. Since the E1M1 term changes sign only with polarization, its finite magnitude leads to an offset in HD curves (Fig. 4b,c).

The E1E2 coupling term is often ignored because it vanishes for random orientation of molecules due to rotational isotropic averaging. However, if the molecules are preferentially aligned, the quadrapolar interactions containing A'' cannot be neglected[39]. This is the case for asymmetric LG beams, in which the spatial inhomogeneity in the intensity profile at the interaction region gives rise to optical dipole force defined by $\mathbf{F} = \alpha\frac{1}{2}\nabla E^2 + \alpha\frac{d}{dt}(\mathbf{E} \times \mathbf{B})$, where the first term defines the gradient force and the second term is the scattering force which can be neglected when the Poynting vector remains constant over an optical cycle. A net non-zero force is exerted on the induced dipoles directed towards the extrema of the radiation field (figure 3a). The resultant torque preferentially aligns the molecular axis parallel to the polarization plane[40] leading to non-zero averaged E1E2 contribution to HD. The E1E2 contribution to HD vanishes for symmetric LG beams since the gradient force is zero. The E1M1 term is non-zero even for randomly oriented molecules.

Assuming full alignment, equation 2 was evaluated for HD(Type I) using the experimental parameters (Eq. 12-19, $\omega = 2.35 \times 10^{15}$ Hz, $\omega_0 = 2\mu m$) and approximating the response tensors G' and A'' with scalars (or pseudoscalar)[41]. Figure 5a depicts the modelled E1E2 term (described in terms of differential optical helicity $\Delta\Upsilon$) for different polarizations described by ellipticity ε. The magnitude of differential absorption is maximum for circular polarization (ε = 1), decreases with ellipticity and goes to zero for perfect linear polarization (ε=0). This is in agreement with the experimentally observed sinusoidal behaviour of Type I: HD for chiral molecule shown in fig. 5b and achiral molecules shown in fig. 3b,c. The minimum ε value achieved experimentally was 0.05. In the experiments, the displacement of singularity is restricted by the focal spot, whereas,

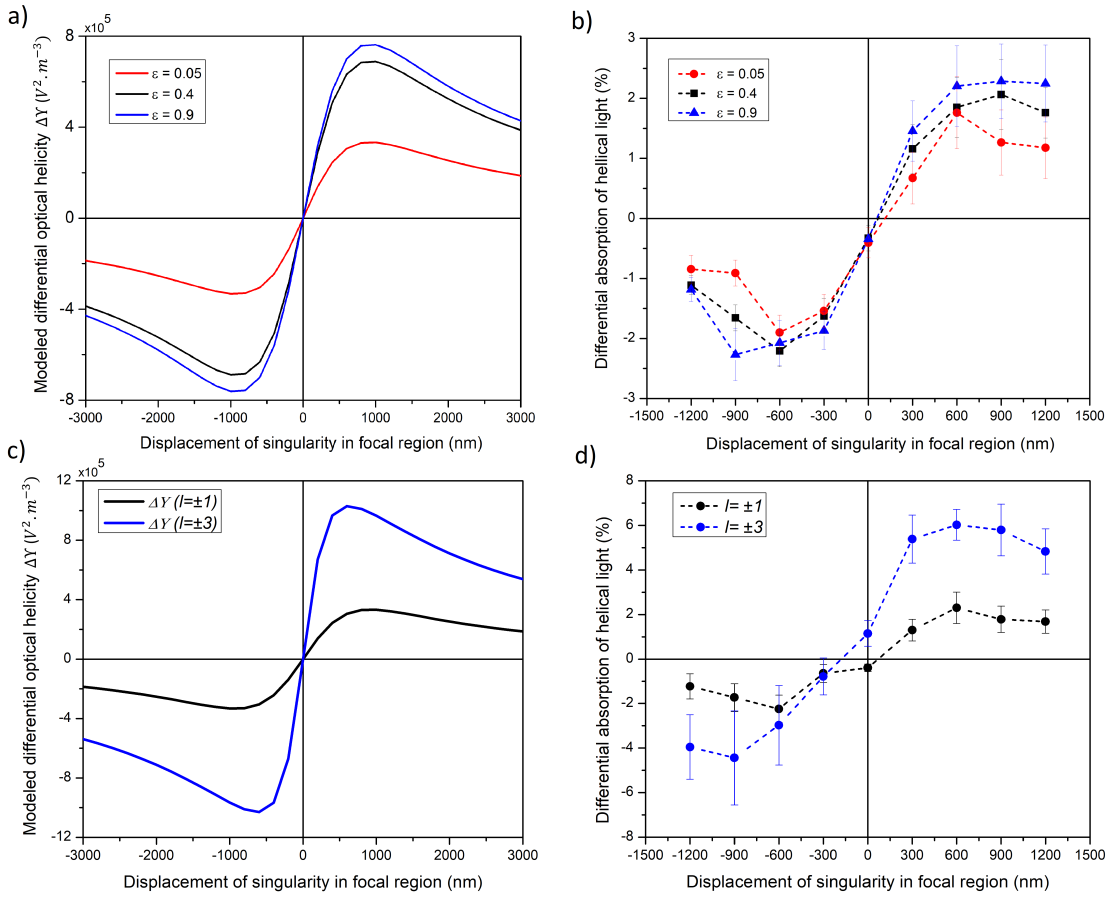

Figure 5. Helical dichroism with asymmetric OAM beams in limonene. Modelled and measured differential absorption as a function of the displacement of singularity **(a,b)** for $l = \pm 1$ and different ellipticities, and **(c,d)** for 95% linearly polarized helical light for $l = \pm 1, \pm 3$. Differential absorption was modelled by the relation $\Delta W \approx A'' \Delta\Upsilon$ where $\Delta\Upsilon = \int_{-\omega_0}^{\omega_0} [\Upsilon^+ - \Upsilon^-] \mathrm{dxdy}$ is differential optical helicity representing the E1E2 coupling term *(see text for details)*.

the modelling of E1E2 term does not include such boundary effects. As a result, at the extreme positions of the singularity in the experiment, the intensity profile mimics a symmetric Gaussian, leading to zero gradient force *(see Supplementary section 8)* and subsequently no differential absorption. However, in the modelling, the intensity profile does not converge to a symmetric Gaussian.

For asymmetric LG beams, the modelled E1E2 term predicts a higher magnitude of differential absorption for higher values of l as shown in Fig. 5c. Figure 5d shows experimental differential absorption, HD(Type I), for asymmetric LG beams in limonene for two different OAM values of $l = \pm 1, \pm 3$. The magnitude of HD increases with the l value in agreement with modelled E1E2 term, where the limonene response tensor is approximated as a scalar quantity. The E1E2 term is non-zero even for asymmetric non-OAM annular beams. However, since there is no l-dependence, differential absorption does not exist, as shown in Fig. 3c for non-OAM, annular beam obtained through Fresnel diffraction.

The contribution of the E1E2 term to the HD signal also depends on the laser fluence. It vanishes at low laser intensity where the degree of molecular alignment is negligible. The extent of molecular alignment with a $\sim$100 fs laser pulse depends on (a) laser intensity ($\sim 10^{13} W/cm^2$), (b) molecular polarizability and (c) temperature and/or solute effects[42–46]. As the laser intensity increases, any degree of alignment in an asymmetric OAM beam is sufficient for the E1E2 term to be non-zero, and its contribution to the HD signal increases as observed in the experiments (Fig. 2, 4b,c).

Our technique affords tunability of OAM dependent differential absorption in both chiral and achiral systems by (i) changing the ellipticity of the laser polarization (Fig. 5a,b), (ii) varying the l-value (Fig. 5c,d), (iii) superimposing Gaussian and OAM beams to manipulate the field distributions, and (iv) shifting the singularity. The technique is quite general and

can be extended to chiral and achiral transparent solids, plasmonic meta-surfaces and gas-phase molecules. OAM of light offers an additional degree of freedom to control light-matter interactions. This opens new opportunities in next-generation chiroptical spectroscopy, asymmetric catalysis and light-driven molecular machines, where ultrashort light pulses can trigger interconversion of enantiomers for dynamic control of chirality.

A key advantage of using helical light is that the HD signal scales linearly with l value, as predicted by our qualitative model. In Fig.5, a linear increase in differential absorption was observed by changing from $l = 1$ to $l = 3$. Our model predicts a linear behaviour until $l \approx 15$; therefore, an increase in differential absorption by a factor of 15 relative to $l = 1$. However, at very high l values a saturation behaviour can be expected, as observed recently in chiral nanostructures[27], due to the increase in the size of the singularity and the finite beam waist determined by the focusing geometry. The enhanced differential absorption with asymmetric OAM beams at higher l-values can be utilized in molecular optical switching for digital processing in which light transmission can be controlled with helicity.

Another unique feature of the scaling behaviour of HD signal is that it leads to higher chiral sensitivity. In contrast, the sensitivity of current chiroptical techniques that rely on light polarization is predetermined by the nature of light-matter interaction, which is not scalable. In fenchone, the chiral signal increased from $\sim$4% to $\sim$6% when l was varied from 1 to 2 (Fig. 2). However, the chiral signal in limonene did not show such dependence. While the l-dependence of the chiral signal needs further investigation, the sensitivity of our technique is comparable to PECD, which to-date has the highest efficiency.

The demonstrated differential absorption in liquids suggests a degree of control over the ionization of gas-phase molecules when irradiated with an intense helical light beam. In addition to polarization and magnetic field, OAM of light represents another parameter to control the continuum trajectory of ionized electrons. OAM of light together with transverse magnetic field and longitudinal electric field generate chiral continuum electrons scalable with l-value. In contrast to chiral electrons created via single photon ionization, chiral electrons generated by tunnel ionization have attosecond resolution and can be used to probe chiral dynamics with attosecond precision.

Finally, the chiral motion of free electrons also results in a magnetic field along the laser propagation axis that can be controlled via the optical OAM. The magnetic field will be dominant around the singular part of the beam where the electric field is weak. For OAM single cycle pulses, the magnetic field can be switched on a time-scale of about 1fs. This opens a potentially new way to in-situ, ultrafast probing of magnetic materials.

Methods

Differential absorption measurements

Ti: Sapphire laser amplifier system, operating in an external trigger mode producing 45 fs, 800 nm pulses with a maximum pulse energy of 2.5 mJ, was used in the transmission measurements. An aspheric objective lens (NA=0.3) was used to focus the femtosecond pulses into a cuvette (10 mm thick) containing liquid samples of chiral or achiral molecules. A second aspheric objective with the same or higher numerical aperture (NA=0.5) collected and collimated the transmitted light onto a photodiode (PD2), positioned immediately after the objective. For every laser shot, the transmitted light signal on PD2 was normalized with the incoming light signal on PD1, reflected off a glass plate positioned in the beam path at an angle of $\sim 20^{\circ}$ to avoid Brewster's angle. The signals generated by PD1 and PD2 were stretched by an electronic pulse stretcher, discretized and recorded by a data acquisition card. A combination of a half-wave plate and a polarizer was used to vary the pulse energy (power control in Fig. 1a). The incident pulse energies were measured before the objective. During the measurement, for every laser shot, the pulse energy was increased by $\sim$ 3nJ and the sample was translated by 5μm to avoid micro-bubbles. Multiple transmission curves similar to Fig. 1a were obtained for each sample to be averaged and smoothed. The difference in the normalized transmission of left- and right-helical light ($l = \pm 1$) is proportional to the differential absorption. To ensure a shortest pulse in the interaction region, a negative chirp was introduced and optimized by measuring the second harmonic generation in a BBO crystal placed at the location of the cuvette. A single-shot auto-correlator then continuously monitored the pulse duration. The pulse duration at the interaction region is about 100fs. Transmission measurements were always performed in an empty cuvette prior to each experiment to determine and minimize background errors resulting from any discrepancies between the photodiodes (*see Supplementary section 5*). In addition, the measured single-shot beam profile, pulse spectrum, and OAM value remained unchanged after transmission through the samples (*see Supplementary sections, 2,3,4*).

Sign dependence of HD in chiral molecules

We used conventional labelling of a chiral molecule by the sign of the direction of rotation of polarized light, *dextrorotatory* $(D;+)$ and *levorotatory* $(L;-)$. Chiral molecules are also labelled as (S)- and (R)- based on absolute chemical configuration representing the left- and right-handed isomers. This labeling refers to the spatial orientation of groups at the chiral center and not to the optical rotation of polarized light. As a result, it is possible for an isomer to be S(+), S(-), R(+) and R(-). The sign dependence of the HD signals arises from two contributing factors: optical rotation by an enantiomer and the topological charge of the q-plates used to generate OAM beams. In fig.2a,b, the HD signals in limonene and fenchone are of opposite signs

because they rotate the plane of linear polarization in opposite directions. R(+)-limonene and S(+)-Fenchone rotate the plane of polarization clockwise while S(-)-limonene and R(-)-Fenchone rotate counter-clockwise. In fig.2b,c the HD signals in fenchone are of opposite signs for $l = \pm 1$ and $l = \pm 2$ because the topological charge of the q-plates used to generate them are of opposite sign, *l=1(q=+1/2)* and *l=2(q=-1)*. This arises because the molecular director of the liquid crystals that make up the q-plate are rotating in opposite directions. As a result, the handedness of light will be flipped, which was not taken into consideration in the plots. This is also the case for limonene (Fig.2a,d) where the topological charges are opposite for *l=1(q=+1/2)* and *l=3(q=-3/2)*.

Generation of OAM beams

Light beams carrying orbital and/or spin angular momentum were generated and controlled by OAM/SAM unit (Fig.1a) consisting of a combination of half- and quarter-wave plates (HWP and QWP), linear polarizer (LP) and a birefringent liquid crystal based phase plate called $q-plate$[31]. When an incident Gaussian beam propagates through the q-plate with a topological charge q, it acquires an OAM defined by $l = \pm 2q$ with a phase singularity and hence a null intensity region at the center of the beam - an optical vortex. The wavefront structure of such beams undergoes l rotations in one wavelength, the direction of rotation is determined by the sign of the input polarization. The conversion efficiency of the q-plates were $91 \pm 2\%$ for $l = 1, 3$ and $\sim 80 \pm 2\%$ for $l = 2$. Circularly (linearly) polarized Gaussian beams were produced by a QWP. The ellipticity of circularly polarized light at the sample was $97 \pm 2\%$. Circularly (linearly) polarized OAM light $s = \pm 1, l = \pm 1$ ($s = 0, l = \pm 1$) was generated using a combination of QWP, q-plate, QWP, LP and QWP. The ellipticity of circularly (linearly) polarized OAM light was $95 \pm 2\%$ ($5 \pm 2\%$) reaching the sample.

Generation of annular beams and displacement of singularity

An annular light beam with no OAM ($l = 0$) was generated by a circular aperture and exploiting the Fresnel diffraction of the incident Gaussian beam to produce an Airy pattern beam with a null region in the center of the beam (*see Supplementary section 6*). A Galilean beam expander and QWP were used to magnify the beam by a factor of 4 and produce circular polarization. The singularity/null intensity region in the OAM (non-OAM beam) beam was displaced by translating the q-plate (circular aperture), mounted on a x,y- stages with a step size of $250 \pm 10 \mu$m. When focused by the objective, this translated to a displacement step size of 300 ± 20nm with respect to the center of the beam. The calibration was achieved by measuring the total translation required to displace the singularity to the periphery of the defocused beam and comparing it to the measured spot size of 2 ± 0.2 μm obtained by knife-edge measurements.

Multipole expansion of light-matter interaction

The induced electric-dipole, $\tilde{\mu}$, electric quadrupole, $\tilde{\theta}$, and magnetic dipole,$\tilde{m}$, are expressed in multipole expansion terms written as[35,47]

$$\tilde{\mu}_\alpha = \sum_\beta \tilde{\alpha}_{\alpha\beta}\tilde{E}_\beta + \sum_\beta \tilde{G}_{\alpha\beta}\tilde{B}_\beta + \frac{1}{3}\sum_{\beta\gamma}\tilde{A}_{\alpha\beta\gamma}\tilde{E}_{\beta\gamma}; \qquad \tilde{\theta}_{\alpha\beta} = \sum_\gamma \tilde{a}_{\gamma\alpha\beta}\tilde{E}_\gamma; \qquad \tilde{m}_\alpha = \sum_\beta \tilde{\chi}_{\alpha\beta}\tilde{B}_\beta + \sum_\beta \tilde{g}_{\alpha\beta}\tilde{E}_\beta \tag{5}$$

where the Greek alphabet represents the Cartesian indices. $\tilde{\alpha}_{\alpha\beta}$ is the electric dipole polarizability, $\tilde{A}_{\alpha\beta\gamma}$ is the electric dipole -quadrupole polarizability, where $\tilde{A}_{\alpha\beta\gamma} = \tilde{a}_{\gamma\alpha\beta}$, and $\tilde{G}_{\alpha\beta}$ is the electric-magnetic dipole polarizability, where $\tilde{G}_{\alpha\beta} = -\tilde{g}_{\alpha\beta}$. The field gradient $\nabla_\beta \tilde{E}_\gamma$ is defined by $\tilde{E}_{\beta\gamma}$.[35,47,48]

The complex fields are defined as $\tilde{E}(t) = \tilde{E}_0 e^{-i\omega t}$ and $\tilde{B}(t) = \tilde{B}_0 e^{-i\omega t}$, where $\tilde{E}_0$ and $\tilde{B}_0$ are arbitrary complex vectors. The terms with tilde are complex quantities $\tilde{\alpha}_{\alpha\beta} = \alpha'_{\alpha\beta} + i\alpha''_{\alpha\beta} = \tilde{\alpha}^*_{\beta\alpha}$, $\tilde{A}_{\alpha\beta\gamma} = A'_{\alpha\beta\gamma} + iA''_{\alpha\beta\gamma} = \tilde{A}_{\gamma\alpha\beta}$, $\tilde{G}_{\alpha\beta} = G'_{\alpha\beta} + iG''_{\alpha\beta}$.

The dynamic multipole interaction Hamiltonian[35,47] is given by

$$H_{int} = -\mu_\alpha E_\alpha - \frac{1}{3}\theta_{\alpha\beta}E_{\alpha\beta} - m_\alpha B_\alpha - ... \tag{6}$$

The rate of change of the Hamiltonian gives the rate of energy absorption by the induced multipoles i.e.[35,47] energy absorbed from the EM fields, expressed in terms of time-average.

$$\Gamma = \langle \dot{\mu}_\alpha E_\alpha + \dot{m}_\alpha B_\alpha + \frac{1}{3}\dot{\theta}_{\alpha\beta}E_{\alpha\beta}\rangle_t \tag{7}$$

where $\dot{\mu}, \dot{m}, \dot{\theta}$, $E_\alpha = \frac{1}{2}\left(\tilde{E}_\alpha e^{-i\omega t} + \tilde{E}^*_\alpha e^{i\omega t}\right)$ and $B_\alpha = \frac{1}{2}\left(\tilde{B}_\alpha e^{-i\omega t} + \tilde{B}^*_\alpha e^{i\omega t}\right)$ are real quantities. By considering the component of dipole moment along the electric field direction, we replace β with α[35] to get,

$$\Gamma_{E1-E1} = \frac{\omega}{4}\alpha''_{\alpha\beta}\left(\tilde{E}^*_\beta\tilde{E}_\alpha + \tilde{E}_\beta\tilde{E}^*_\alpha\right) \rightarrow \Gamma_{E1-E1} = \frac{\omega}{2}\alpha''_{\alpha\alpha}\left[\tilde{E}_\alpha\tilde{E}^*_\alpha\right] \tag{8}$$

Magnetic dipole-dipole excitation (M1-M1) is given by

$$\Gamma_{M1-M1} = \frac{\omega}{4}\chi''_{\alpha\beta}\left(\tilde{B}_\beta\tilde{B}^*_\alpha + \tilde{B}^*_\beta\tilde{B}_\alpha\right) \rightarrow \Gamma_{M1-M1} = \frac{\omega}{2}\chi''_{\alpha\alpha}\left[\tilde{B}_\alpha\tilde{B}^*_\alpha\right] \tag{9}$$

Electric-magnetic dipole excitation (E1-M1) results in the interaction of the electric field with the electric dipole moment induced by the magnetic field and *vice-versa*. The expression is given by

$$\Gamma_{E1-M1} = \frac{i\omega}{4}\langle G'_{\alpha\beta}\rangle_\rho\left(\tilde{B}_\beta\tilde{E}^*_\alpha - \tilde{E}_\alpha\tilde{B}^*_\beta\right) \rightarrow \Gamma_{E1-M1} = \frac{\omega}{2}\rho G'_{\alpha\alpha}\mathrm{Im}\left[\tilde{E}^*_\alpha\tilde{B}_\alpha\right] \tag{10}$$

To describe the bulk response, the tensor quantity $G'_{\alpha\beta}$ must be averaged over all degrees of molecular orientation. For partial orientation of molecules, due to the laser induced dipole force, we consider anisotropic averaging $\langle G'_{\alpha\beta}\rangle_\rho \rightarrow \rho G'_{\alpha\alpha}$, where ρ is an orientation-dependent weighting factor influenced by the degree of molecular alignment[49,50].

Electric dipole-quadrupole excitation (E1-E2) arises from two contributions. First, the interaction of the electric field with the electric dipole moment induced by the field gradient. Second, the interaction of the field gradient with the quadrupole moment induced by the electric field. The expression is given by

$$\Gamma_{E1-E2} = \frac{\omega}{6}\langle A''_{\alpha\beta\gamma}\rangle_\rho\left[\nabla_\beta\tilde{E}_\gamma\tilde{E}^*_\alpha + \tilde{E}_\alpha\nabla_\beta\tilde{E}^*_\gamma\right] \rightarrow \Gamma_{E1-E2} = \frac{\omega}{3}\rho A''_{\alpha\alpha\gamma}\mathrm{Re}\left[\tilde{E}^*_\alpha\nabla_\alpha\tilde{E}_\gamma\right] \tag{11}$$

We consider anisotropic averaging $\langle A''_{\alpha\beta\gamma}\rangle_\rho \rightarrow \rho A''_{\alpha\alpha\gamma}$, where ρ is an orientation-dependent weighting factor influenced by the degree of molecular alignment. For complete alignment ($\rho = 1$), considering the principal molecular axis is oriented along the propagation axis (γ), the tensor quantity can be expressed as $\langle A''_{\alpha\beta\gamma}\rangle_\rho \rightarrow \left(A''_{\alpha\alpha\gamma} + A''_{\beta\beta\gamma}\right)$[35]. Since the dominant contribution to the dipole moment is along the electric field direction (α), we limit to $A''_{\alpha\alpha\gamma}$. This tensor quantity vanishes for randomly oriented molecules, $\rho = 0$ (isotropic averaging). The contribution of E1E2 term was modelled in Fig. 5 by considering the optical helicity term Υ and approximating A'' as a scalar. The higher multipole transitions such as E1M2, E2M1, and E2E2 are ignored because the molecular response tensor for these transitions is very small. The total rate of excitation is a sum of all four absorption rates given in equation 1.

Asymmetric Laguerre-Gaussian beams

We introduced an asymmetry parameter, δ, in the symmetric LG beam to obtain an asymmetric LG beam. We also consider the longitudinal component of the field (E_z) as a correction to the paraxial regime[51,52] to take into account its finite l (OAM) contribution. The importance of longitudinal component in light-matter interaction has been recently demonstrated in differentiating nanoparticle aggregates using helical light[26]. When light is focused tightly using a higher NA objective, the contribution of the longitudinal component becomes significant.

For arbitrary polarization in the paraxial regime, the field components can be written as

$$u^{\pm}_o(x,y,z) = E_0\exp[ikz]\left(\frac{\sqrt{2}\left((x\mp i\eta\delta)\pm i(y\mp i\delta)\right)}{\omega_0}\right)^{|l|}\exp\left(-\frac{(x^2+y^2)}{\omega_0^2}\right)L^{|(l+j)|}_{p-j}\left(\frac{2\rho^2}{w_0^2}\right) \tag{12}$$

$$E^{\pm}_x(x,y,z) = \alpha_z u^{\pm}_0(x,y,z) \tag{13}$$

$$E^{\pm}_y(x,y,z) = \beta_z u^{\pm}_0(x,y,z) \tag{14}$$

$$E^{\pm}_z(x,y,z) = if\left[(\alpha_z \pm i\beta_z)\frac{|l|\omega_0((x\mp i\eta\delta)\mp i(y\mp i\delta)}{(x\mp i\eta\delta)^2+(y\mp i\delta)^2}u^{\pm}_0(x,y,z) - \frac{2}{\omega_0}\left(\alpha_z(x)+\beta_z(y)\right)u^{\pm}_0(x,y,z)\right] \tag{15}$$

$$B_x(x,y,z) = -\beta_z\frac{k}{\omega}u^{\pm}_0(\mathbf{r}), \tag{16}$$

$$B_y(x,y,z) = \alpha_z\frac{k}{\omega}u^{\pm}_0(\mathbf{r}) \tag{17}$$

$$B_z(x,y,z) = if\frac{k}{\omega}\left[(\alpha_z \pm i\beta_z)\frac{|l|\omega_0((y\mp i\delta)\pm i(x\mp i\eta\delta))}{(x\mp i\eta\delta)^2+(y\mp i\delta)^2}u^{\pm}_0(\mathbf{r}) - \frac{2}{\omega_0}\left(\alpha_z(y)-\beta_z(x)\right)u^{\pm}_0(\mathbf{r})\right] \tag{18}$$

where $\mathbf{f} = \lambda/2\pi\omega_0$, $\rho = \sqrt{x^2+y^2}$. Also, E_0 is the normalization factor obtained by integrating the intensity over all space (-∞ to + ∞), for (l = 1) it is given as :

$$E_0 = \sqrt{\frac{p!}{(p+|l|)!}}\sqrt{\frac{2k^2\omega_0^2}{\pi\left(\alpha^2+\beta^2\right)\left(2\omega_0^2+k^2\omega_0^4+2\left(1+\eta^2\right)\delta^2\left(1+k^2\omega_0^2\right)\right)}} \tag{19}$$

In our case, there is no radial node, hence p=0. The $\pm$ represents the rotational direction of l. The polarization factors α and β are normalized such that $|\alpha_z|^2 + |\beta_z|^2 = 1$. Displacement of singularity in the x-y plane can be achieved by varying η. For generalization, we substituted $\eta = 1/4$, considering the movement of singularity is slightly displaced from the axial direction experimentally.

References

1. Caldwell, D.J. & Eyring, H., *The Theory of Optical Activity* 244 (University of Utah, Salt Lake City, 1971)

2. Nakanishi, K., Berova, N., & Woody, R., *Circular dichroism: principles and applications* (John Wiley Sons ISBN: 978-0-471-33003-5, 2000).

3. Janssen, M. H. M., & Powis, I., Detecting chirality in molecules by imaging photoelectron circular dichroism. *Phys. Chem. Chem. Phys.* **16**, 856-871 (2014).

4. Tang, Y. & Cohen, A. E., Enhanced enantioselectivity in excitation of chiral molecules by superchiral light. *Science*. **332**, 6027, 333-336 (2011).

5. Collins, J.T., et al. Chirality and chiroptical effects in metal nanostructures: fundamental and current trends. *Adv. Opt. Matter*. **5**, 1700182 (2017).

6. Wang, X. & Tang, Z., Circular dichroism studies on plasmonic nanostructures. *Small*. **13**, 1601115, (2017).

7. Cireasa, R. et al. Probing molecular chirality on a sub-femtosecond timescale. *Nature Phys*. **11**, 654–658 (2015).

8. Bégin, J-L., Alsaawy, M., & Bhardwaj, R., Chiral discrimination by recollision enhanced femtosecond laser mass spectrometry. *Scientific Reports*. **10**, 14074 (2020).

9. Lux, C. et al. Circular dichroism in the photoelectron angular distributions of camphor and fenchone from multiphoton ionization with femtosecond laser pulses. *Angew. Chem. Int. Ed.* **51**, 5001–5005 (2012).

10. Powis, I., Photoelectron circular dichroism of the randomly oriented chiral molecules glyceraldehyde and lactic acid. *J. Chem. Phys.* **112**, 301 (2000).

11. Allen, L. et al. Orbital angular momentum of light and the transformation of Laguerre-Gaussian laser modes. *Phys. Rev. A*. **45**, 8185, (1992).

12. Torres, J.P., & Torner, L., *Twisted Photons: applications of Light with Orbital Angular Momentum* (Wiley, 2011).

13. Andrews, D. L., & Babiker, M., *The Angular Momentum of Light* (Cambridge University Press, 2013).

14. Surzhykov, A., Seipt, D., & Fritzsche, S., Probing the energy flow in Bessel light beams using atomic photoionization. *Phys. Rev. A*. **94**, 033420 (2016).

15. Wätzel, J., & Berakdar, J., Discerning on a sub-optical-wavelength the attosecond time delays in electron emission from magnetic sublevels by optical vortices. *Phys. Rev. A*. **94**, 033414 (2016).

16. Picón, A. et al. Transferring orbital and spin angular momenta of light to atoms.*New J. Phys*. **12**, 083053 (2010).

17. Peshkov, A.A., Fritzsche, S., & Surzhykov, A., Ionization of H_2^+ molecular ions by twisted Bessel light. *Phys. Rev. A*. **92**, 043415 (2015).

18. Franke-Arnold, S., Allen L., & Padgett M., Advances in optical angular momentum. *Laser & photonics Rev*. **2**, 299-313 (2008).

19. Andersen M. F. et al. Quantized rotation of atoms from photons with orbital angular momentum. *Phys. Rev. Lett*. **97**, 170406 (2006).

20. He, H. et al. Direct observation of transfer of angular momentum to absorptive particles from a laser beam with a phase singularity. *Phys. Rev. Lett*. **75**, 826–829 (1995).

21. Schmiegelow, C.T. et al. Transfer of optical orbital angular momentum to a bound electron. *Nat. Commun.*. **7**, 129998 (2016).

22. Picón, A. et al. Photoionization with orbital angular momentum beams. *Optics Express*. **18**, 4, 3660-3671 (2010).

23. Loffler, W., Broer, D. J., & Woerdman, J. P., Circular dichroism of cholesteric polymers and the orbital angular momentum of light. *Phys. Rev. A*. **83**, 065801 (2011).

24. Araoka, F., et al. Interactions of twisted light with chiral molecules: an experimetal investigation. *Phys. Rev. A*. **71**, 055401 (2005).

25. Andrews, D. L., Romero, L. D., & Babiker, M., On optical vortex interactions with chiral matter. *Opt. Commun*. **237** 133–139 (2004).

26. Brullot, W. et al. Resolving enantiomers using the optical angular momentum of twisted light. *Science Advances*. **2**, 150134 (2016).

27. Ni, J. et al. Giant Helical dichroism of single chiral nanostructures with photonic orbital angular momentum. *ACs Nano*. **15**, 2, 2893-2900, (2021).

28. Forbes, K. A., & Andrews, D. L., Spin-orbit interactions and chiroptical effects engaging orbital angular momentum of twisted light in chiral and achiral media. *Phys. Rev. A* **99** 023837 (2019)

29. Forbes, K. A., & Andrews, D. L., Optical orbital angular momentum: twisted light and chirality. Opt. Lett. **43** 435-438 (2018).

30. Oosterbeek, R., Ashforth, S., Bodley, O., & Simpson, M., Measuring the ablation threshold fluence in femtosecond laser micromachining with vortex and Bessel pulses. *Opt. Express* **26**, 34558-34568 (2018).

31. Marrucci, L., Manzo, C., & Paparo, D., Optical Spin-to-Orbital Angular Momentum Conversion in Inhomogeneous Anisotropic Media. *Phys. Rev. Lett.*, **96**, 163905 (2006).

32. Hugo, L. et al. Arbitrary optical wavefront shaping via spin-to-orbit coupling. *J. Opt*. **18**, 124002 (2016).

33. Rahimian, M.G. et al. Spatially controlled nano-structuring of silicon with femtosecond vortex pulses. *Sci Rep* **10**, 12643 (2020).

34. Lipkin, D., Existence of a New Conservation Law in Electromagnetic Theory. *J. Math. Phys. (N.Y.)* **5**, 696-700 (1964).

35. Yang, N., & Cohen, A.E., Local Geometry of Electromagnetic Fields and Its Role in Molecular Multipole Transitions. *Journal of Physical Chemistry B* , **115**, (18),5304-5311 (2011).

36. Wang, Z. et al. A Novel Chiral Metasurface with Controllable Circular Dichroism Induced by Coupling Localized and Propagating Modes. *Adv. Opt. Mater.*. **4**, 883-8 (2016).

37. Guo, Y. et al. Orbital angular momentum dichroism caused by the interaction of electric and magnetic dipole moments and the geometrical asymmetry of chiral metal nanoparticles. *Phys. Rev. A* **102**, 033525 (2020).

38. Loudon, R.*The Quantum Theory of Light*. (Oxford University Press, 2003).

39. Forbes, K. A., & Andrews, D. L., Orbital angular momentum of twisted light: chirality and optical activity. *J. Phys. Photonics* **3**, 022007 (2021).

40. Bradshaw, D. S, & Andrews, D. L., Manipulating particles with light: radiation and gradient forces. *Eur. J. Phys.* **38**, 034008 (2017).

41. Tang, Y., & Cohen, A. E., Optical Chirality and Its Interaction with Matter. *Phys. Rev. Lett.* **104**, 163901 (2010).

42. Ohkubo, J. et al,. Molecular alignment in a liquid induced by a nonresonant laser field: Molecular dynamics simulation. *J. Chem. Phys.* **120**, 9123 (2004).

43. Dooley, P. W. et al. Direct imaging of rotation wave-packet dynamics of diatomic molecules. *Phys. Rev. A* **68**, 023406 (2003).

44. Fleischer, S. et al. Molecular Alignment Induced by Ultrashort Laser Pulses and Its Impact on Molecular Motion. *Is. J. of Chem.*. **52** (5) :414-437, (2012).

45. Leibscher, M., Averbukh, I.S., & Rabitz H., Molecular Alignment by Trains of Short Laser Pulses. *Phys. Rev. Lett.* **90**, 213001 (2003).

46. Leibscher, M., Averbukh, I. S., & Rabitz H., Enhanced molecular alignment by short laser pulses. *Phys. Rev. A* **69**, 013402 (2004).

47. Barron, L. D., *Molecular Light Scattering and Optical Activity* (Cambridge University Press, Cambridge, England, 2004).

48. Buckingham, A.D., & Dunn, M. B., Optical Activity of Oriented Molecules. *J. Chem. Soc. (A)*, 1988-1991 (1971).

49. Andrews, S.S., Using rotational averaging to calculate the bulk response of isotropic and anisotropic samples from molecular parameters. *J. Chem. Educ.*, **81**, 6, 877 (2004).

50. Andrews, D. L., & Allcock, P., *Optical harmonics in molecular systems: quantum electrodynamical theory* (John Wiley & Sons ISBN: 978-3-527-60274-2, 2005).

51. Cerjan, A. et al. Orbital angular momentum of Laguerre–Gaussian beams beyond the paraxial approximation. *J. Opt. Soc. Am. A.*, **28**, 2253-2260 (2011).

52. Forbes, K. A. et al. Relevance of longitudinal fields of paraxial optical vortices. *J. Opt.* **23** 075401 (2021).

Acknowledgements (not compulsory)

Author contributions statement

J-L.B., A.J. and R.B., conceived the experiments. J-L.B., A.J. and R.B. designed and planned the experiments. J-L.B. and A.J. conducted the experiments and analyzed the results. J-L.B, A.J, A.P., T.B. and R.B. worked on the theory and conducted numerical simulations. F.H fabricated the q-plates, P.C, E.K., and R.B. supervised the project. J-L.B., A.J., T.B. and R.B. prepared the first draft and all authors reviewed the manuscript.

Additional information

To include, in this order: **Accession codes** (where applicable); **Competing interests** (mandatory statement).

The corresponding author is responsible for submitting a competing interests statement on behalf of all authors of the paper. This statement must be included in the submitted article file.

Supplementary Files

This is a list of supplementary files associated with this preprint. Click to download.

- SupplementaryScalablenonlinearhelicaldichroisminchiralandachiralmolecules.pdf